
B-XAIC Dataset: Benchmarking Explainable AI for Graph Neural Networks Using Chemical Data

Magdalena Proszewska
University of Edinburgh
m.proszewska@ed.ac.uk

Tomasz Danel
Jagiellonian University,
Faculty of Mathematics and Computer Science
Jagiellonian University, Faculty of Chemistry
tomasz.danel@uj.edu.pl

Dawid Rymarczyk
Jagiellonian University,
Faculty of Mathematics and Computer Science
Ardigen SA
dawid.rymarczyk@uj.edu.pl

Abstract

Understanding the reasoning behind deep learning model predictions is crucial in cheminformatics and drug discovery, where molecular design determines their properties. However, current evaluation frameworks for Explainable AI (XAI) in this domain often rely on artificial datasets or simplified tasks, employing data-derived metrics that fail to capture the complexity of real-world scenarios and lack a direct link to explanation faithfulness. To address this, we introduce B-XAIC, a novel benchmark constructed from real-world molecular data and diverse tasks with known ground-truth rationales for assigned labels. Through a comprehensive evaluation using B-XAIC, we reveal limitations of existing XAI methods for Graph Neural Networks (GNNs) in the molecular domain. This benchmark provides a valuable resource for gaining deeper insights into the faithfulness of XAI, facilitating the development of more reliable and interpretable models.

1 Introduction

Graph Neural Networks (GNNs) have become the standard for predictive modeling of small molecules [40], achieving exceptional performance across property prediction, virtual screening, and related pharmaceutical tasks. While their predictive capabilities are well-established, a growing emphasis is now placed on understanding their reasoning [16]. In scientific applications of deep learning to small molecules, transparent explanation mechanisms are not merely desirable but crucial. They build researcher trust, ensure model reliability, and potentially uncover novel insights that can accelerate drug discovery and materials design [43].

To address this gap, a range of Explainable AI (XAI) techniques have been adapted or specifically designed for GNNs, aiming to reveal the mechanisms behind their predictions [16, 17]. These approaches generally fall into two categories: counterfactual methods [8, 21, 37], which seek to identify minimal input changes that alter a model’s prediction, and factual methods [22, 31, 45], which aim to highlight important substructures within the input graph. Factual methods further diverge into post-hoc explainers [45], that analyze a trained black-box model, and inherently interpretable architectures [14, 38, 50], which aim for transparency through their design. However, recent findings indicate a critical challenge: regardless of the specific XAI method used, the resulting explanations can be unreliable, or even misleading, potentially interfering with scientific understanding [13].

Despite the strong performance of these models on established benchmarks and metrics for GNNs and small molecules, this is still observable.

In response to the limitations of current XAI evaluation for GNNs, the community has developed synthetic datasets [2, 4, 22, 42, 45]. However, these often lack real-world complexity, while creating real-world datasets with ground truth explanations is challenging or impossible. Existing real-world datasets like MUTAG are small and task-limited. Furthermore, many evaluation methods rely on thresholding importance maps or selecting top-k elements, which can be problematic for tasks dependent on the presence/absence of substructures, where no single element is inherently more important. This arbitrary selection can yield inaccurate explanations and misleading metrics. While AUROC [6, 49] avoids thresholding, it becomes ineffective when no specific element is important, leading to empty ground truth explanations.

To address these limitations, we introduce B-XAIC (Benchmark for eXplainable Artificial Intelligence in Chemistry), a novel benchmark comprising 50K small molecules and 7 diverse tasks, accompanied by both ground truth labels and corresponding explanations, making accuracy-based metrics a directly applicable and reliable evaluation method. B-XAIC tackles the challenges associated with thresholding explanations or selecting the top-k most important elements by considering two distinct scenarios: (1) cases where a specific part of the input graph constitutes the explanation, which can be effectively evaluated using AUROC or Average Precision (AP), and (2) cases where the entire graph is equally important for the prediction, in which the evaluation focuses on ensuring the explanation does not contain irrelevant outliers. Ultimately, B-XAIC enables a direct and fair comparison of various factual XAI approaches, both post-hoc explainers and inherently self-explainable models.

2 Related Work

Explainability in GNNs. Recent research in Graph Neural Networks (GNNs) has increasingly focused on developing methods to interpret and explain the decisions made by these models. Explainable AI (XAI) techniques for GNNs can be broadly categorized based on the type of explanation they provide [17]. These methods may involve identifying key substructures within the input graph that influence the model’s predictions, offering factual explanations by highlighting relevant parts of the input [10, 22, 45, 48], or generating counterfactual examples where the input is perturbed in such a way that it leads to a different prediction outcome [8, 21, 37].

Furthermore, factual methods for explaining GNN predictions can be broadly classified into post-hoc and self-interpretable approaches. Post-hoc methods aim to explain the predictions of a pre-trained GNN by identifying important nodes, edges, or features that influence the model’s decision [22, 31, 45]. In contrast, self-interpretable methods design the GNN architecture to inherently incorporate explainability using information constraints, such as attention blocks [27, 38] or bottlenecks [41], or integrating structural constraints like prototypes [29, 50] or graph kernels [9, 14], to ensure that the model is more interpretable by design.

Explainability Benchmarks. The need for appropriate datasets to evaluate GNN explainability techniques has led to the introduction of various benchmark datasets with ground-truth explanations. Several synthetic datasets have been developed for node classification and graph classification tasks, where specific motifs serve as the ground truth. For instance, datasets like BA-Shapes, BA-Community, Tree Cycle, and Tree Grids [45] are designed for node classification, with the task of predicting whether a node is part of a known motif (such as a cycle, house, or grid). Similarly, synthetic datasets like BA-2Motifs [22], BAMultiShapes [4] and Spurious Motifs [42] are designed for graph classification tasks, where the goal is to detect presence of given motifs in the entire graph.

ShapeGGen [2] is a more recent development in the field of graph benchmarks. It is a synthetic graph generator designed to create a variety of graph datasets with diverse characteristics. While ShapeGGen provides valuable synthetic data, it remains limited by its artificial nature, which may not fully capture the complexity and noise present in real-world datasets.

In addition to synthetic datasets, real-world datasets have been crucial for testing GNN explainability methods. Molecular datasets are particularly valuable in this context, as they can provide ground-truth explanations based on known chemical properties. Examples of such datasets include MUTAG [11], Benzene, Fluoride-Carbonyl, and Alkane-Carbonyl [26, 30], which are graph classification tasks where explanations are based on the presence or absence of simple chemical structures: the

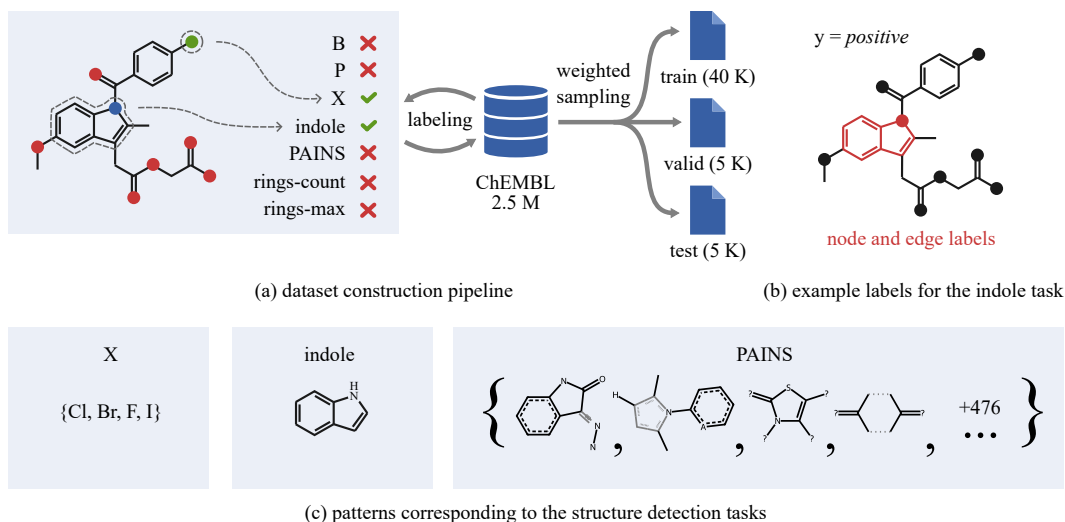


Figure 1: Schematic of our B-XAIC dataset and benchmark; (a) the dataset preparation steps include compound labeling, filtering, and sampling to the training, validation, and testing subsets; (b) for each positive example, atom and bond labels are provided to assess model explanations; (c) the patterns for the halogen and indole tasks are presented, as well as four example PAINS patterns

NO_2 group in MUTAG, the benzene ring in Benzene, fluoride (F^-) and carbonyl ($\text{C}=\text{O}$) groups in Fluoride-Carbonyl, and alkane (F^-) and carbonyl ($\text{C}=\text{O}$) groups in Alkane-Carbonyl. These datasets contain 1.8K, 12K, 8.7K and 1.1K graphs, respectively. Although simple, these datasets serve as effective benchmarks and are commonly used in the field.

Furthermore, many XAI GNN methods are evaluated on more complex molecular datasets where ground-truth explanations are not available, such as NC11 [39], BBBP [24], Tox21 [25], or Proteins [7]. In addition to these, several domain-specific GNN benchmarks are used to assess explainability and related metrics in fields such as visual recognition, natural language processing, or fairness. In the visual domain, datasets like MNIST-75sp [19] transform images into graphs, where each superpixel is treated as a graph node to test GNN systems. In the textual domain, datasets like Graph SST2, Graph SST5, and Graph Twitter [47] convert sentiment analysis datasets into graph-structured data, allowing for the evaluation of GNN explainability in natural language processing tasks. In the fairness domain, social graph datasets like German Credit, Recidivism, and Credit Defaulter are used to evaluate fairness when dealing with sensitive data [1]. These domain-specific benchmarks provide valuable insights into how GNNs can be interpreted across various applications, thereby expanding the scope and relevance of XAI research. However, since ground-truth explanations are often either unavailable or inherently impossible to define, the evaluation of explainability in these contexts shifts from accuracy-based measures to other aspects of XAI systems [28], such as fidelity [3, 20, 51], sparsity [21, 46], sufficiency, necessity [8, 37], or robustness [6]. These metrics typically evaluate how predicted explanations or predicted classes change in response to alterations in the input graph.

Recognizing the need for more robust evaluation, we developed the B-XAIC benchmark. This resource comprises 50,000 diverse examples with 7 tasks, each paired with ground truth explanations that reflect the intricacies of real-world applications. Our evaluation proceeds in two stages: initially, we determine if a method correctly identifies instances with no significant nodes; subsequently, we examine its accuracy in highlighting the relevant subgraph. Fully covering current challenges in benchmarking XAI methods for GNNs.

3 Benchmark

In this section, firstly we will introduce the B-XAIC dataset that is the core of our benchmark, and then we will provide details on how to evaluate explanations using B-XAIC.

3.1 Dataset Construction

Our benchmark dataset was sourced from ChEMBL 35 [15], which is a public database of 2.5 M molecules with drug-like properties shared under the CC BY-SA 3.0 license. The molecules were pre-filtered by removing invalid or duplicated SMILES strings. The solvent molecules and counterions were removed to keep only one molecular graph per example.

The benchmark tasks are based on the presence of chemical substructures (see Figure 1), with increasing difficulty of chemical patterns:

1. Detection of organoboron and organophosphorus compounds. The goal of these two tasks is to predict if a compound contains a boron (B) or phosphorus (P) atom, respectively.
2. Detection of halogens (X). The prediction should be positive if any of the halogen atoms (bromine, chlorine, fluorine, and iodine) are present in the molecule. This task verifies whether GNNs can find one of multiple alternative patterns in the graph.
3. Detection of indoles, a bicyclic structure with a benzene ring fused to a pyrrole ring. Compounds containing this structure are widely distributed in nature. In this task, a GNN should effectively pass messages between nodes to detect a larger pattern in the graph.
4. Detection of pan-assay interference compounds (PAINS). Some chemical structures tend to produce false-positive results in high-throughput screens. We use the list of such patterns proposed by Baell and Holloway [5]. This task aims to test whether a GNN is able to learn multiple more complex patterns.
5. Counting rings. The model should predict if a molecule contains more than four rings. This task involves both detecting a pattern and counting its occurrences.
6. Detecting large rings with more than six atoms. This task involves counting nodes within a substructure.

The final dataset is produced by sampling 50 K molecules from the pre-filtered ChEMBL dataset. Weighted sampling is used to avoid huge class imbalance. The weights are defined as the product of the ratios between the majority and minority classes for all tasks. The average size of a graph in the resulting dataset is 34.56. The data is split randomly into training, validation, and testing sets using the 8-1-1 ratio. The dataset contains a set of binary task labels for each compound and two sets of explanation labels, one for the atoms and one for the edges involved in each detected pattern. Figure 2 illustrates the diversity of the graphs in the dataset.

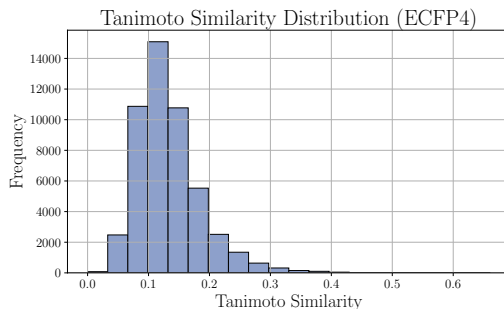


Figure 2: Histogram of Tanimoto similarities illustrating the diversity of the dataset.

3.2 Evaluation Metrics

For each task and each graph, the ground truth explanation is defined as a subset of nodes and edges that are relevant to the task.

These explanations fall into two categories:

- **Null explanations (NE)** – where no nodes or edges are more important than others. For example, in task B, if atom B is not present in the graph, then no specific substructure can be considered relevant.
- **Subgraph explanations (SE)** – where only a part of the graph is relevant to the task. For instance, in task B, if atom B is present, that node constitutes the explanation.

We evaluate these two groups separately:

- **Null explanations:** The predicted explanation should be uniform for all nodes and edges, without highlighting specific substructures as more important. This requirement can be

formally restated as no outliers among the node and edge explanations. To measure this, we use the interquartile range (IQR) method. A prediction is assigned a score of 1 if no outliers are detected, and 0 otherwise.

- **Subgraph explanations:** Because it may be difficult to find the optimal threshold for explanation methods to extract all relevant nodes or edges, we rely on the AUROC metric to test if the most significant nodes and edges are prioritized over the remaining graph structure.

This evaluation is done separately for node-based and edge-based explanations. Table 1 contains relevant details.

Table 1: Summary of Task and Dataset Statistics. SE denotes relevant subgraphs in positive instances, while NE denotes negative instances without explanations.

task	% of graphs with positive label	% of graphs with NE	% of nodes in SE	% of edges in SE
B	2.18	97.78	4.13 ± 2.16	–
P	12.78	86.71	4.35 ± 2.44	–
X	56.46	44.13	6.05 ± 4.07	–
indole	36.94	63.33	31.34 ± 12.15	31.49 ± 12.16
PAINS	32.88	67.08	34.07 ± 14.22	31.37 ± 14.63
rings-count	30.06	1.49	64.04 ± 16.03	61.85 ± 14.84
rings-max	5.54	1.35	50.22 ± 17.44	47.12 ± 16.39

4 Results

4.1 Experimental setup

Explainers. We evaluate a range of explanation methods for graph neural networks, including both gradient-based and mask-based approaches. GNNExplainer [45] learns a soft mask over the input graph to identify important substructures, while PGExplainer [22] is a parametric version that generalizes across instances. IntegratedGradients [36], Saliency [33], and Input×Gradient [32] are gradient-based methods that attribute importance to input features based on their sensitivity. Deconvolution [23, 32] and GuidedBackprop [34] refine backpropagation to highlight relevant features more clearly. GraphMask [31] uses reinforcement learning to learn sparse binary masks, and ShapleyValueSampling [35] approximates feature importance via Shapley values. We assess both node- and edge-based explanations depending on the capabilities of each method.

Models. We apply explainers to several popular graph neural network architectures: GCN [18], GAT [38], GIN [44], and ProtGNN [50], a prototype-based, inherently interpretable GNN, instantiated with GCN, GAT, and GIN backbones. We primarily report results for GIN, with missing results for GCN, GAT, and ProtGNN variants provided in the Appendix.

We conduct our experiments using an NVIDIA H100 GPU with 80GB of HBM3 memory.

Table 2: F1 scores obtained by three GNN architectures and ProtGNN using these architectures as its backbone; the highest scores are highlighted in bold along with the numbers that are not significantly lower according to the one-sided Wilcoxon test

	GCN	ProtGNN +GCN	GAT	ProtGNN +GAT	GIN	ProtGNN +GIN
B	99.94 ± 0.05	97.38 ± 1.42	99.11 ± 0.19	98.52 ± 1.69	99.96 ± 0.05	96.98 ± 0.69
P	99.98 ± 0.02	95.52 ± 7.98	99.97 ± 0.01	99.51 ± 0.22	99.98 ± 0.03	99.77 ± 0.14
X	99.84 ± 0.05	99.68 ± 0.05	99.18 ± 0.23	99.89 ± 0.05	99.94 ± 0.02	98.74 ± 0.56
indole	88.33 ± 1.74	73.80 ± 16.62	67.30 ± 2.21	76.17 ± 2.52	98.32 ± 0.36	95.76 ± 0.89
PAINS	79.89 ± 0.47	56.34 ± 5.57	65.02 ± 1.65	54.27 ± 0.64	92.90 ± 0.54	85.88 ± 4.26
rings-count	87.27 ± 1.61	68.74 ± 8.31	82.88 ± 0.59	71.04 ± 4.89	99.62 ± 0.21	83.48 ± 0.69
rings-max	91.25 ± 1.13	91.63 ± 0.19	91.03 ± 0.79	91.63 ± 0.18	92.98 ± 0.84	91.63 ± 0.19

Table 3: Evaluation of the node and edge explanations for the GIN model; the explainers are grouped into three categories: gradient-based (GB), graph-specific (GS), and perturbation-based (PB); the best score and all scores not significantly lower according to the one-sided Wilcoxon test are highlighted in bold

Class	Explainer	nodes			edges		
		NE	SE	avg	NE	SE	avg
GB	Saliency	0.52 ± 0.13	0.82 ± 0.17	0.67	0.33 ± 0.17	0.61 ± 0.11	0.47
	Deconvolution	0.74 ± 0.14	0.54 ± 0.28	0.64	0.45 ± 0.16	0.55 ± 0.18	0.50
	InputXGradient	0.54 ± 0.14	0.71 ± 0.25	0.62	0.39 ± 0.18	0.56 ± 0.10	0.48
	GuidedBackprop	0.41 ± 0.12	0.84 ± 0.13	0.62	0.37 ± 0.11	0.65 ± 0.15	0.51
	IntegratedGradients	0.39 ± 0.27	0.72 ± 0.27	0.56	0.35 ± 0.17	0.57 ± 0.17	0.46
GS	GNNExplainer	0.69 ± 0.12	0.54 ± 0.10	0.61	0.57 ± 0.12	0.52 ± 0.03	0.54
	GraphMaskExplainer	0.66 ± 0.03	0.50 ± 0.01	0.58	0.36 ± 0.05	0.50 ± 0.00	0.43
	PGExplainer	-	-	-	0.05 ± 0.06	0.37 ± 0.16	0.21
PB	ShapleyValueSampling	0.47 ± 0.24	0.71 ± 0.27	0.59	0.22 ± 0.11	0.55 ± 0.12	0.39

4.2 Benchmarking

Our benchmark evaluation incorporates multiple GNN architectures, with classification metrics for the designated tasks presented in Table 2. While all evaluated methods demonstrate strong F1 scores across most tasks, GIN consistently outperforms alternative architectures.

As anticipated, the detection of PAINS patterns emerges as the most challenging task, requiring the identification of various alert substructures. Several architectures also exhibit limitations in recognizing indole rings, suggesting insufficient capacity to capture extensive substructures within molecular graphs. The ring-counting task similarly presents difficulties for most models, particularly ProtGNN, which is not capable of highlighting disconnected molecular fragments [12].

Given our benchmark’s primary focus on comparing XAI methods, subsequent analysis will emphasize results from the GIN architecture, which achieves near-perfect performance across our synthetic tasks. This exceptional performance suggests that GIN formulates predictions based on appropriate chemical principles, making it an ideal candidate for our explainability evaluations.

Node explanations. First, we will focus on node explanations. Table 3 shows the results of various XAI methods applied to GIN, our best-performing model. The reported evaluation metrics are averaged across all tasks, and all best results that are not statistically significantly worse than the highest number (according to a one-sided Wilcoxon test) are highlighted in bold. Gradient-based methods are, on average, better at localizing important patterns than other methods. However, they tend to highlight molecular fragments even when the pattern is absent, resulting in low NE scores.

The detailed results for each task are shown in Figure 3 and further detailed in the Appendix. Two groups of explanation methods are formed. The first one achieves good NE scores and obtains lower SE scores, and the other group exhibits opposite behavior. This suggests that some methods provide

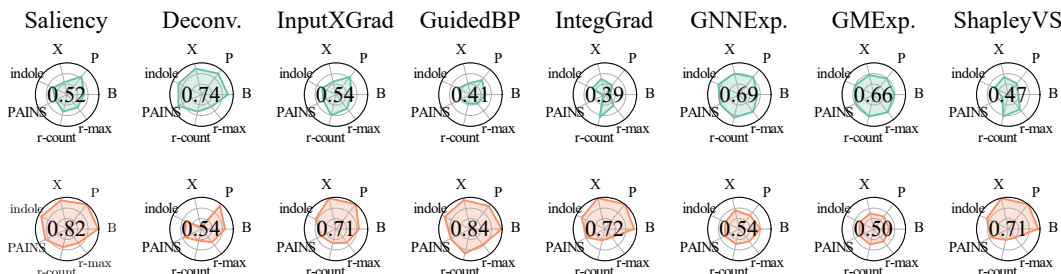


Figure 3: Evaluation of node-level explanations for GIN. Null explanation results are shown in green, and subgraph explanation results in orange. Overall average scores for each method are displayed in the center.

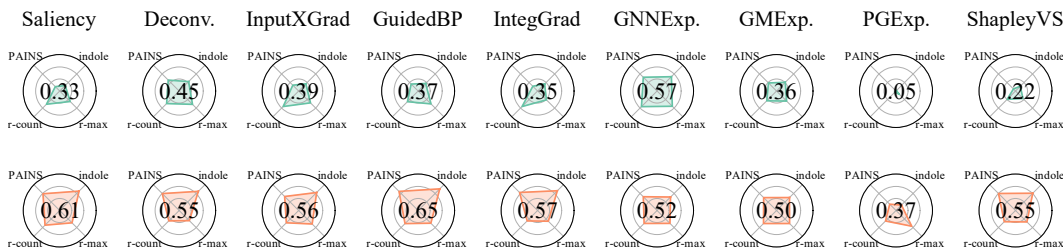


Figure 4: Evaluation of edge-level explanations for GIN. Null explanation results are shown in green, and subgraph explanation results in orange. Overall average scores for each method are displayed in the center.

more contrastive and precise explanations, while other methods return more uniform attributions. The tasks of finding boron, phosphorus, and halogen atoms are the easiest for all the methods. The most difficult patterns to find are those related to rings, either counting them or measuring their size.

Edge explanations. Similar analysis was conducted for edges, and the results are shown in Table 3. In this case, gradient-based methods do not always outperform the other methods in terms of the SE metric. The strong performance of the methods based on subgraph extraction may be caused by the fact that edges are included in the extracted subgraphs, while gradient methods often focus more on nodes. Interestingly, the GNNExplainer model significantly outperforms all other methods in the NE metric, while GuidedBackprop is best at detecting important edges (one-sided Wilcoxon test).

The results of all explainers are presented in Figure 4, and the exact numbers can be found in the Appendix. In these results, we focus on four tasks that involve edges, excluding all tasks aiming at detecting single atoms. Also in the case of edges, tasks related to counting rings or atoms in rings appear to be more challenging for the explainers.

Relationship between model performance and explanation quality. As illustrated in Figure 5, there exists a notable correlation between model performance and the quality of the explanations generated for prediction outcomes. This relationship is particularly evident in more complex tasks, such as PAINS detection, where SE scores are correlated with F1 scores. The data suggests that models achieving superior predictive accuracy also tend to produce more meaningful structural explanations. In contrast, the correlation between model performance and NE scores appears considerably weaker.

Explanation examples Figure 6 illustrates representative explanations for both positive and negative graph instances. We observe that some techniques tend to highlight atoms proximal to the relevant subgraph, potentially due to limited control over the message-passing mechanism in GNNs. Additionally, we observe that even methodologically similar explanation approaches can generate markedly divergent explanations for the same graph. For the negative instances, there is no universal threshold that can be used across all methods to separate important nodes because one method can attribute weights near zero uniformly for all the nodes, while another method predicts uniform values around 4.5. In both cases no subgraph can be highlighted as predicted to be more significant. All these observations lead to the conclusion that widely used explainers struggle to highlight even simple patterns for GNNs that achieve almost perfect accuracy. This emphasizes the immense need for benchmarks like B-XAIC to accelerate research on new XAI methods for graphs.

4.3 Discussion

Our findings clearly demonstrate the critical need for new XAI benchmarks specifically tailored to molecular graphs. Current XAI techniques exhibit significant deficiencies in generating adequate explanations, even for the most elementary tasks proposed in our B-XAIC benchmark. Despite the GIN model achieving remarkably high performance metrics, with F1 scores exceeding 98% for all proposed tasks, the explanations generated by the explainers consistently fail to properly identify and highlight the relevant molecular structures.

While complex nonlinear interactions between atoms undoubtedly characterize real-world chemical applications, our benchmark reveals that incorrect atom attribution persists even in comparatively

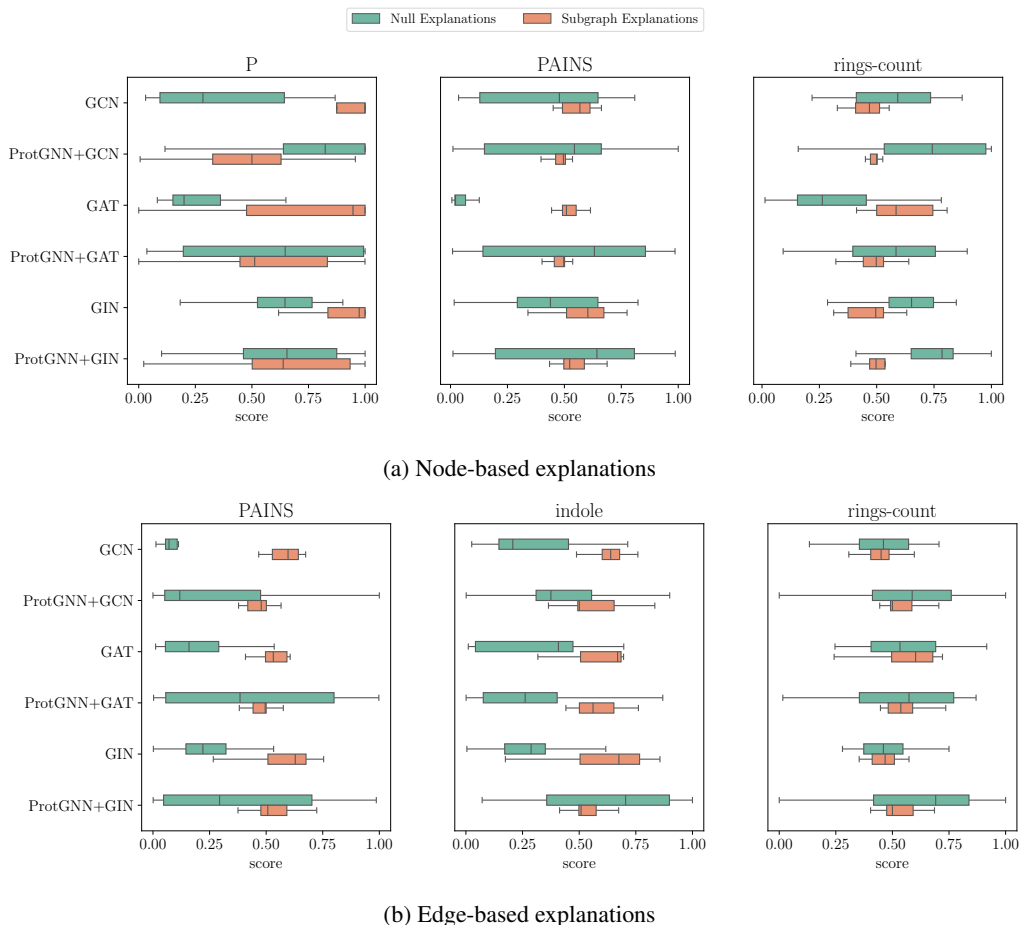


Figure 5: Boxplots showing the distribution of explanation quality across different explainers for each model. Results are aggregated per model, highlighting that some models are inherently more difficult to explain than others.

simple tasks. This systematic failure likely stems from the fundamental architectural principles underlying GNNs. The iterative message-passing layers inherent to these networks result in information diffusion among neighboring nodes, substantially impeding precise localization of salient features. This phenomenon represents a significant challenge to the field and warrants focused investigation into novel approaches that can maintain predictive power while enhancing interpretability.

Limitations. The primary limitation of this study lies in its exclusive focus on local explanations. This design choice is justified by the current landscape of GNN explainability methods, where support for global explanations remains limited, hindering a direct and fair comparison across diverse techniques. Furthermore, the utilization of real-world molecular data, while providing real-world data complexity, introduces a potential confound. We cannot definitively guarantee that the trained models base their predictions on the intended underlying chemical principles. Consequently, suboptimal performance of an XAI method on B-XAIC could be attributed to either deficiencies in the explanation technique itself or from the model’s failure to learn the task based on the expected structural features. Therefore, a holistic evaluation of explainer performance, considering both explanation quality metrics and the model’s predictive accuracy on the test set, is crucial when utilizing this benchmark.

Broader Impact. This work contributes to the broader field of explainable AI (XAI), specifically within the context of graph neural networks applied to drug discovery and molecular modeling. The B-XAIC dataset offers the community a standardized benchmark for evaluating novel XAI techniques dedicated to small molecules. Beyond this specific domain, we anticipate its utility for assessing XAI methods on graphs of moderate size (up to 60 nodes), a common scale in various

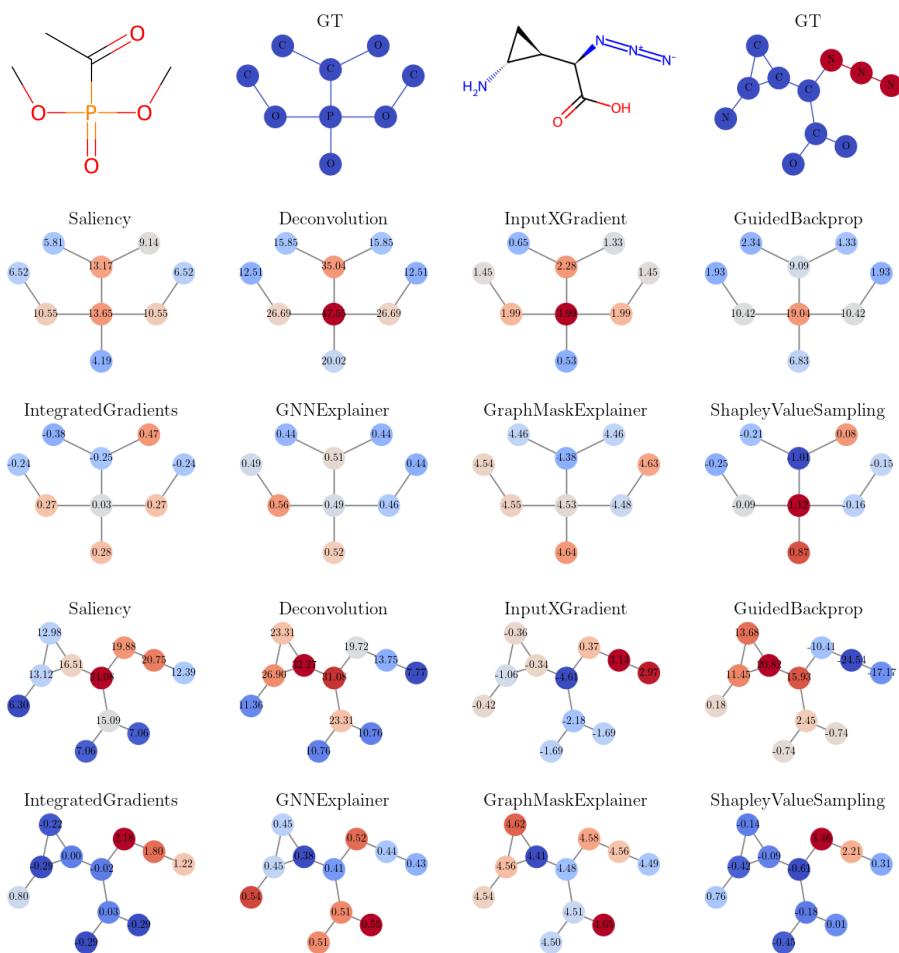


Figure 6: Node-level explanation examples on graphs from different classes in the PAINS task, using the GIN model and different explanation methods.

real-world applications. More generally, this research provides a valuable example for the broader XAI community, demonstrating how real-world data and carefully designed tasks of increasing complexity can be leveraged for effective and insightful XAI benchmarking. Ultimately, we envision that B-XAIC will facilitate the development of more robust and transparent XAI methods for graph data. This advancement holds a promise to enhance the interpretability and trustworthiness of GNNs, allowing for their wider adoption in critical production environments, especially in scientific discovery and the design of new therapeutics.

Safeguards, licencing and open access to data and code. To ensure accessibility and encourage community engagement, we have hosted the B-XAIC dataset on Hugging Face and provided open-source code for its execution. Furthermore, the careful design of our molecule selection process and data hosting infrastructure allows us to effectively mitigate the risk of data misuse. Importantly, the dataset is released under the CC-BY-SA license, empowering the community to leverage this resource while ensuring proper attribution and continued sharing. You can find the data and code under the following links: <https://huggingface.co/datasets/mproszewska/B-XAIC>, <https://github.com/mproszewska/B-XAIC>.

5 Conclusions

In conclusion, the B-XAIC dataset offers a valuable new resource for the GNN XAI community. By providing real-world molecular data with structure-derived ground truth explanations, our dataset enables rigorous benchmarking of both inherently interpretable graph models and post-hoc GNN explainers. The introduction of null and subgraph explanation concepts, along with the edge-based and node-based variations, offers a more nuanced evaluation of XAI capabilities across different explanation types and graph aspects. We believe B-XAIC will serve as a crucial baseline for future research, clearly highlighting the strengths and limitations of emerging XAI methods.

Our ongoing work aims to further enrich this dataset by incorporating activity-cliff scenarios, pushing the boundaries of XAI techniques to uncover subtle but critical distinctions within graph data.

Acknowledgements

We thank Jacek Tabor and Marek Śmieja for helpful discussions at early stages of this project.

The work of T. Danel was funded by "Interpretable and Interactive Multimodal Retrieval in Drug Discovery" project. The „Interpretable and Interactive Multimodal Retrieval in Drug Discovery” project (FENG.02.02-IP.05-0040/23) is carried out within the First Team programme of the Foundation for Polish Science co-financed by the European Union under the European Funds for Smart Economy 2021-2027 (FENG).

The work of D. Rymarczyk was funded by National Centre of Science (Poland) grant no. 2023/49/B/ST6/01137.

Some experiments were performed on servers purchased with funds from the Priority Research Area (Artificial Intelligence Computing Center Core Facility) under the Strategic Programme Excellence Initiative at Jagiellonian University.

References

- [1] Chirag Agarwal, Himabindu Lakkaraju, and Marinka Zitnik. Towards a unified framework for fair and stable graph representation learning. In Cassio P. de Campos, Marloes H. Maathuis, and Erik Quaeghebeur, editors, *Proceedings of the Thirty-Seventh Conference on Uncertainty in Artificial Intelligence, UAI 2021, Virtual Event, 27-30 July 2021*, volume 161 of *Proceedings of Machine Learning Research*, pages 2114–2124. AUAI Press, 2021.
- [2] Chirag Agarwal, Owen Queen, Himabindu Lakkaraju, and Marinka Zitnik. Evaluating explainability for graph neural networks. *Scientific Data*, 10(144), 2023.
- [3] Kenza Amara, Rex Ying, Zitao Zhang, Zhihao Han, Yinan Shan, Ulrik Brandes, Sebastian Schemm, and Ce Zhang. Graphframex: Towards systematic evaluation of explainability methods for graph neural networks, 2022.
- [4] Steve Azzolin, Antonio Longa, Pietro Barbiero, Pietro Liò, and Andrea Passerini. Global explainability of gnns via logic combination of learned concepts. In *The Eleventh International Conference on Learning Representations, ICLR 2023, Kigali, Rwanda, May 1-5, 2023*. OpenReview.net, 2023.
- [5] Jonathan B Baell and Georgina A Holloway. New substructure filters for removal of pan assay interference compounds (pains) from screening libraries and for their exclusion in bioassays. *Journal of medicinal chemistry*, 53(7):2719–2740, 2010.
- [6] Mohit Bajaj, Lingyang Chu, Zi Yu Xue, Jian Pei, Lanjun Wang, Peter Cho-Ho Lam, and Yong Zhang. Robust counterfactual explanations on graph neural networks. In Marc’Aurelio Ranzato, Alina Beygelzimer, Yann N. Dauphin, Percy Liang, and Jennifer Wortman Vaughan, editors, *Advances in Neural Information Processing Systems 34: Annual Conference on Neural Information Processing Systems 2021, NeurIPS 2021, December 6-14, 2021, virtual*, pages 5644–5655, 2021.
- [7] Karsten M. Borgwardt, Cheng Soon Ong, Stefan Schönauer, S. V. N. Vishwanathan, Alex J. Smola, and Hans-Peter Kriegel. Protein function prediction via graph kernels. *Bioinformatics*, 21(1):47–56, 2005.
- [8] Ziheng Chen, Fabrizio Silvestri, Jia Wang, Yongfeng Zhang, Zhenhua Huang, Hongshik Ahn, and Gabriele Tolomei. Grease: Generate factual and counterfactual explanations for gnn-based recommendations, 2022.

- [9] Luca Cosmo, Giorgia Minello, Alessandro Bicciato, Michael M. Bronstein, Emanuele Rodolà, Luca Rossi, and Andrea Torsello. Graph kernel neural networks. *IEEE Transactions on Neural Networks and Learning Systems*, 36(4):6257–6270, April 2025.
- [10] Enyan Dai and Suhang Wang. Towards self-explainable graph neural network, 2021.
- [11] Asim Kumar Debnath, Rosa L. Lopez de Compadre, Gargi Debnath, Alan J. Shusterman, and Corwin Hansch. Structure-activity relationship of mutagenic aromatic and heteroaromatic nitro compounds. correlation with molecular orbital energies and hydrophobicity. *Journal of Medicinal Chemistry*, 34(2):786–797, 1991.
- [12] Khawla Elhadri, Tomasz Michalski, Adam Wróbel, Jörg Schlötterer, Bartosz Zieliński, and Christin Seifert. This looks like what? challenges and future research directions for part-prototype models. *ArXiv preprint*, abs/2502.09340, 2025.
- [13] Lukas Faber, Amin K. Moghaddam, and Roger Wattenhofer. When comparing to ground truth is wrong: On evaluating GNN explanation methods. In Feida Zhu, Beng Chin Ooi, and Chunyan Miao, editors, *KDD '21: The 27th ACM SIGKDD Conference on Knowledge Discovery and Data Mining, Virtual Event, Singapore, August 14-18, 2021*, pages 332–341. ACM, 2021.
- [14] Aosong Feng, Chenyu You, Shiqiang Wang, and Leandros Tassioulas. Kergnns: Interpretable graph neural networks with graph kernels. In *Thirty-Sixth AAAI Conference on Artificial Intelligence, AAAI 2022, Thirty-Fourth Conference on Innovative Applications of Artificial Intelligence, IAAI 2022, The Twelfth Symposium on Educational Advances in Artificial Intelligence, EAAI 2022 Virtual Event, February 22 - March 1, 2022*, pages 6614–6622. AAAI Press, 2022.
- [15] Anna Gaulton, Louisa J Bellis, A Patricia Bento, Jon Chambers, Mark Davies, Anne Hersey, Yvonne Light, Shaun McGlinchey, David Michalovich, Bissan Al-Lazikani, et al. ChEMBL: a large-scale bioactivity database for drug discovery. *Nucleic acids research*, 40(D1):D1100–D1107, 2012.
- [16] José Jiménez-Luna, Francesca Grisoni, and Gisbert Schneider. Drug discovery with explainable artificial intelligence. *Nature Machine Intelligence*, 2(10):573–584, 2020.
- [17] Jaykumar Kakkad, Jaspal Jannu, Kartik Sharma, Charu Aggarwal, and Sourav Medya. A survey on explainability of graph neural networks, 2023.
- [18] Thomas N. Kipf and Max Welling. Semi-supervised classification with graph convolutional networks. In *5th International Conference on Learning Representations, ICLR 2017, Toulon, France, April 24-26, 2017, Conference Track Proceedings*. OpenReview.net, 2017.
- [19] Boris Knyazev, Graham W. Taylor, and Mohamed R. Amer. Understanding attention and generalization in graph neural networks. In Hanna M. Wallach, Hugo Larochelle, Alina Beygelzimer, Florence d’Alché-Buc, Emily B. Fox, and Roman Garnett, editors, *Advances in Neural Information Processing Systems 32: Annual Conference on Neural Information Processing Systems 2019, NeurIPS 2019, December 8-14, 2019, Vancouver, BC, Canada*, pages 4204–4214, 2019.
- [20] Antonio Longa, Steve Azzolin, Gabriele Santin, Giulia Cencetti, Pietro Lio, Bruno Lepri, and Andrea Passerini. Explaining the explainers in graph neural networks: a comparative study. *ACM Computing Surveys*, 57(5):1–37, January 2025.
- [21] Ana Lucic, Maartje A. ter Hoeve, Gabriele Tolomei, Maarten de Rijke, and Fabrizio Silvestri. Cf-gnnexplainer: Counterfactual explanations for graph neural networks. In Gustau Camps-Valls, Francisco J. R. Ruiz, and Isabel Valera, editors, *International Conference on Artificial Intelligence and Statistics, AISTATS 2022, 28-30 March 2022, Virtual Event*, volume 151 of *Proceedings of Machine Learning Research*, pages 4499–4511. PMLR, 2022.
- [22] Dongsheng Luo, Wei Cheng, Dongkuan Xu, Wenchao Yu, Bo Zong, Haifeng Chen, and Xiang Zhang. Parameterized explainer for graph neural network. In Hugo Larochelle, Marc’ Aurelio Ranzato, Raia Hadsell, Maria-Florina Balcan, and Hsuan-Tien Lin, editors, *Advances in Neural Information Processing Systems 33: Annual Conference on Neural Information Processing Systems 2020, NeurIPS 2020, December 6-12, 2020, virtual*, 2020.
- [23] Aravindh Mahendran and Andrea Vedaldi. Salient deconvolutional networks. In Bastian Leibe, Jiri Matas, Nicu Sebe, and Max Welling, editors, *Computer Vision – ECCV 2016*, pages 120–135, Cham, 2016. Springer International Publishing.
- [24] Ines Filipa Martins, Ana L. Teixeira, Luis Pinheiro, and Andre O. Falcao. A bayesian approach to in silico blood-brain barrier penetration modeling. *Journal of Chemical Information and Modeling*, 52(6):1686–1697, 2012. PMID: 22612593.

- [25] Andreas Mayr, Günter Klambauer, Thomas Unterthiner, and Sepp Hochreiter. Deeptox: Toxicity prediction using deep learning. *Frontiers in Environmental Science*, Volume 3 - 2015, 2016.
- [26] Kevin McCloskey, Ankur Taly, Federico Monti, Michael P. Brenner, and Lucy J. Colwell. Using attribution to decode binding mechanism in neural network models for chemistry. *Proceedings of the National Academy of Sciences*, 116(24):11624–11629, 2019.
- [27] Siqi Miao, Mia Liu, and Pan Li. Interpretable and generalizable graph learning via stochastic attention mechanism. In Kamalika Chaudhuri, Stefanie Jegelka, Le Song, Csaba Szepesvári, Gang Niu, and Sivan Sabato, editors, *International Conference on Machine Learning, ICML 2022, 17-23 July 2022, Baltimore, Maryland, USA*, volume 162 of *Proceedings of Machine Learning Research*, pages 15524–15543. PMLR, 2022.
- [28] Meike Nauta, Jan Trienes, Shreyasi Pathak, Elisa Nguyen, Michelle Peters, Yasmin Schmitt, Jörg Schlöterer, Maurice van Keulen, and Christin Seifert. From anecdotal evidence to quantitative evaluation methods: A systematic review on evaluating explainable ai. *ACM Computing Surveys*, 55(13s):1–42, July 2023.
- [29] Dawid Rymarczyk, Daniel Dobrowolski, and Tomasz Danel. ProgreSt: Prototypical graph regression soft trees for molecular property prediction. In *Proceedings of the 2023 SIAM International Conference on Data Mining (SDM)*, pages 379–387. SIAM, 2023.
- [30] Benjamin Sanchez-Lengeling, Jennifer N. Wei, Brian K. Lee, Emily Reif, Peter Wang, Wesley Wei Qian, Kevin McCloskey, Lucy J. Colwell, and Alexander B. Wiltschko. Evaluating attribution for graph neural networks. In Hugo Larochelle, Marc’Aurelio Ranzato, Raia Hadsell, Maria-Florina Balcan, and Hsuan-Tien Lin, editors, *Advances in Neural Information Processing Systems 33: Annual Conference on Neural Information Processing Systems 2020, NeurIPS 2020, December 6-12, 2020, virtual*, 2020.
- [31] Michael Sejr Schlichtkrull, Nicola De Cao, and Ivan Titov. Interpreting graph neural networks for NLP with differentiable edge masking. In *9th International Conference on Learning Representations, ICLR 2021, Virtual Event, Austria, May 3-7, 2021*. OpenReview.net, 2021.
- [32] Avanti Shrikumar, Peyton Greenside, Anna Shcherbina, and Anshul Kundaje. Not just a black box: Learning important features through propagating activation differences, 2016.
- [33] Karen Simonyan, Andrea Vedaldi, and Andrew Zisserman. Deep inside convolutional networks: Visualising image classification models and saliency maps, 2014.
- [34] Jost Tobias Springenberg, Alexey Dosovitskiy, Thomas Brox, and Martin Riedmiller. Striving for simplicity: The all convolutional net, 2015.
- [35] Erik Štrumbelj and Igor Kononenko. An efficient explanation of individual classifications using game theory. *J. Mach. Learn. Res.*, 11:1–18, 2010.
- [36] Mukund Sundararajan, Ankur Taly, and Qiqi Yan. Axiomatic attribution for deep networks. In Doina Precup and Yee Whye Teh, editors, *Proceedings of the 34th International Conference on Machine Learning, ICML 2017, Sydney, NSW, Australia, 6-11 August 2017*, volume 70 of *Proceedings of Machine Learning Research*, pages 3319–3328. PMLR, 2017.
- [37] Juntao Tan, Shijie Geng, Zuohui Fu, Yingqiang Ge, Shuyuan Xu, Yunqi Li, and Yongfeng Zhang. Learning and evaluating graph neural network explanations based on counterfactual and factual reasoning. In *Proceedings of the ACM Web Conference 2022, WWW ’22*. ACM, April 2022.
- [38] Petar Velickovic, Guillem Cucurull, Arantxa Casanova, Adriana Romero, Pietro Liò, and Yoshua Bengio. Graph attention networks. In *6th International Conference on Learning Representations, ICLR 2018, Vancouver, BC, Canada, April 30 - May 3, 2018, Conference Track Proceedings*. OpenReview.net, 2018.
- [39] Nikil Wale and George Karypis. Comparison of descriptor spaces for chemical compound retrieval and classification. In *Sixth International Conference on Data Mining (ICDM’06)*, pages 678–689, 2006.
- [40] Oliver Wieder, Stefan Kohlbacher, Méline Kuenemann, Arthur Garon, Pierre Ducrot, Thomas Seidel, and Thierry Langer. A compact review of molecular property prediction with graph neural networks. *Drug Discovery Today: Technologies*, 37:1–12, 2020.
- [41] Tailin Wu, Hongyu Ren, Pan Li, and Jure Leskovec. Graph information bottleneck. In Hugo Larochelle, Marc’Aurelio Ranzato, Raia Hadsell, Maria-Florina Balcan, and Hsuan-Tien Lin, editors, *Advances in Neural Information Processing Systems 33: Annual Conference on Neural Information Processing Systems 2020, NeurIPS 2020, December 6-12, 2020, virtual*, 2020.

- [42] Yingxin Wu, Xiang Wang, An Zhang, Xiangnan He, and Tat-Seng Chua. Discovering invariant rationales for graph neural networks. In *The Tenth International Conference on Learning Representations, ICLR 2022, Virtual Event, April 25-29, 2022*. OpenReview.net, 2022.
- [43] Zhenxing Wu, Jihong Chen, Yitong Li, Yafeng Deng, Haitao Zhao, Chang-Yu Hsieh, and Tingjun Hou. From black boxes to actionable insights: a perspective on explainable artificial intelligence for scientific discovery. *Journal of Chemical Information and Modeling*, 63(24):7617–7627, 2023.
- [44] Keyulu Xu, Weihua Hu, Jure Leskovec, and Stefanie Jegelka. How powerful are graph neural networks? In *7th International Conference on Learning Representations, ICLR 2019, New Orleans, LA, USA, May 6-9, 2019*. OpenReview.net, 2019.
- [45] Zhitao Ying, Dylan Bourgeois, Jiaxuan You, Marinka Zitnik, and Jure Leskovec. Gnnexplainer: Generating explanations for graph neural networks. In Hanna M. Wallach, Hugo Larochelle, Alina Beygelzimer, Florence d’Alché-Buc, Emily B. Fox, and Roman Garnett, editors, *Advances in Neural Information Processing Systems 32: Annual Conference on Neural Information Processing Systems 2019, NeurIPS 2019, December 8-14, 2019, Vancouver, BC, Canada*, pages 9240–9251, 2019.
- [46] Junchi Yu, Jie Cao, and Ran He. Improving subgraph recognition with variational graph information bottleneck, 2021.
- [47] Hao Yuan, Haiyang Yu, Shurui Gui, and Shuiwang Ji. Explainability in graph neural networks: A taxonomic survey, 2020.
- [48] Hao Yuan, Haiyang Yu, Jie Wang, Kang Li, and Shuiwang Ji. On explainability of graph neural networks via subgraph explorations. In Marina Meila and Tong Zhang, editors, *Proceedings of the 38th International Conference on Machine Learning, ICML 2021, 18-24 July 2021, Virtual Event*, volume 139 of *Proceedings of Machine Learning Research*, pages 12241–12252. PMLR, 2021.
- [49] Yue Zhang, David Defazio, and Arti Ramesh. Relex: A model-agnostic relational model explainer, 2020.
- [50] Zaixi Zhang, Qi Liu, Hao Wang, Chengqiang Lu, and Cheekong Lee. Protgnn: Towards self-explaining graph neural networks. In *Thirty-Sixth AAAI Conference on Artificial Intelligence, AAAI 2022, Thirty-Fourth Conference on Innovative Applications of Artificial Intelligence, IAAI 2022, The Twelveth Symposium on Educational Advances in Artificial Intelligence, EAAI 2022 Virtual Event, February 22 - March 1, 2022*, pages 9127–9135. AAAI Press, 2022.
- [51] Xu Zheng, Farhad Shirani, Tianchun Wang, Wei Cheng, Zhuomin Chen, Haifeng Chen, Hua Wei, and Dongsheng Luo. Towards robust fidelity for evaluating explainability of graph neural networks. In *The Twelfth International Conference on Learning Representations, ICLR 2024, Vienna, Austria, May 7-11, 2024*. OpenReview.net, 2024.

A Full Evaluation Results

Here we provide the full set of results that were shown partially in the main paper. These results accompany the introduction of our benchmark and offer a detailed view of node and edge explanation performance across different explainer types.

A.1 Ranking by evaluation scores

Table 4 and Table 5 report the evaluation metrics for all model–explainer combinations, averaged across tasks and sorted by the aggregated scores for node and edge explanations, respectively.

A.2 Visual summary of evaluation scores

The radar plots in Figure 7 and Figure 8 illustrate the evaluation scores of each model–explainer combination across all 7 tasks, providing a visual comparison of their performance.

A.3 Visualization of correlation between evaluation metrics and model performance

Figure 9 compare NE and SE metrics for each evaluated model and illustrate the correlation between evaluation scores and model performance for each task.

A.4 Examples of explanations

Figures 10–16 present examples of node explanations for the GIN classifier for each task using the evaluated explainers. The colors in the null explanations are scaled to highlight outlier scores based on the IQR method applied in our evaluation. Specifically, scores below $Q1 - 1.5 \times IQR$ or above $Q3 + 1.5 \times IQR$ are considered outliers, where $Q1$ and $Q3$ represent the 25th and 75th percentiles, respectively, and $IQR = Q3 - Q1$.

Table 4: Ranking of all model–explainer combinations based on the evaluation of **node explanations**, sorted by overall scores. The best score and all scores not significantly lower (according to a one-sided Wilcoxon test) are highlighted in bold. For NE and SE, we report the mean and standard deviation; for the overall score (avg), we additionally provide the standard error of the mean (SEM) to highlight the trade-off between NE and SE performance.

Model	Explainer	NE	SE	avg
ProtGNN+GIN	Saliency	0.64±0.21	0.74±0.24	0.69±0.05
ProtGNN+GIN	GuidedBackprop	0.80±0.27	0.58±0.18	0.69±0.11
ProtGNN+GCN	GuidedBackprop	0.90±0.16	0.46±0.16	0.68±0.22
GIN	Saliency	0.52±0.13	0.82±0.17	0.67±0.15
GCN	Deconvolution	0.73±0.16	0.61±0.29	0.67±0.06
ProtGNN+GAT	Saliency	0.56±0.35	0.75±0.21	0.66±0.09
GIN	Deconvolution	0.74±0.14	0.54±0.28	0.64±0.10
ProtGNN+GIN	GNNExplainer	0.75±0.18	0.53±0.09	0.64±0.11
ProtGNN+GCN	GNNExplainer	0.77±0.17	0.49±0.07	0.63±0.14
ProtGNN+GIN	Deconvolution	0.73±0.17	0.53±0.26	0.63±0.10
GIN	InputXGradient	0.54±0.14	0.71±0.25	0.62±0.09
ProtGNN+GAT	GNNExplainer	0.71±0.18	0.54±0.08	0.62±0.08
GIN	GuidedBackprop	0.41±0.12	0.84±0.13	0.62±0.22
GIN	GNNExplainer	0.69±0.12	0.54±0.10	0.61±0.07
ProtGNN+GCN	Deconvolution	0.76±0.14	0.47±0.25	0.61±0.14
GCN	GuidedBackprop	0.53±0.21	0.69±0.28	0.61±0.08
GCN	Saliency	0.46±0.13	0.76±0.25	0.61±0.15
ProtGNN+GAT	GuidedBackprop	0.75±0.34	0.46±0.20	0.61±0.14
ProtGNN+GCN	Saliency	0.64±0.22	0.56±0.24	0.60±0.04
GIN	ShapleyValueSampling	0.47±0.24	0.71±0.27	0.59±0.12
GCN	GraphMaskExplainer	0.67±0.04	0.50±0.01	0.58±0.08
ProtGNN+GAT	GraphMaskExplainer	0.67±0.04	0.50±0.01	0.58±0.08
ProtGNN+GCN	GraphMaskExplainer	0.67±0.04	0.50±0.01	0.58±0.08
GAT	GraphMaskExplainer	0.67±0.04	0.50±0.01	0.58±0.08
ProtGNN+GIN	GraphMaskExplainer	0.66±0.03	0.50±0.01	0.58±0.08
GIN	GraphMaskExplainer	0.66±0.03	0.50±0.01	0.58±0.08
GIN	IntegratedGradients	0.39±0.27	0.72±0.27	0.56±0.17
GCN	GNNExplainer	0.55±0.15	0.53±0.08	0.54±0.01
ProtGNN+GIN	IntegratedGradients	0.44±0.25	0.63±0.18	0.53±0.09
GAT	GNNExplainer	0.32±0.17	0.69±0.21	0.51±0.19
GCN	ShapleyValueSampling	0.27±0.17	0.73±0.26	0.50±0.23
ProtGNN+GIN	InputXGradient	0.55±0.27	0.45±0.19	0.50±0.05
GCN	InputXGradient	0.25±0.20	0.74±0.26	0.49±0.24
ProtGNN+GAT	InputXGradient	0.51±0.38	0.42±0.24	0.47±0.05
GCN	IntegratedGradients	0.19±0.18	0.74±0.25	0.46±0.28
ProtGNN+GAT	IntegratedGradients	0.43±0.35	0.49±0.26	0.46±0.03
GAT	Saliency	0.19±0.21	0.72±0.24	0.46±0.26
ProtGNN+GIN	ShapleyValueSampling	0.25±0.24	0.65±0.18	0.45±0.20
ProtGNN+GCN	ShapleyValueSampling	0.25±0.28	0.57±0.21	0.41±0.16
ProtGNN+GCN	IntegratedGradients	0.30±0.28	0.52±0.19	0.41±0.11
GAT	Deconvolution	0.24±0.23	0.57±0.32	0.40±0.17
GAT	GuidedBackprop	0.24±0.23	0.57±0.32	0.40±0.17
ProtGNN+GCN	InputXGradient	0.38±0.31	0.42±0.21	0.40±0.02
GAT	ShapleyValueSampling	0.26±0.22	0.49±0.34	0.38±0.12
GAT	IntegratedGradients	0.24±0.22	0.50±0.35	0.37±0.13
ProtGNN+GAT	Deconvolution	0.25±0.17	0.49±0.25	0.37±0.12
GAT	InputXGradient	0.25±0.23	0.47±0.37	0.36±0.11
ProtGNN+GAT	ShapleyValueSampling	0.21±0.31	0.49±0.22	0.35±0.14

Table 5: Ranking of all model–explainer combinations based on the evaluation of **edge explanations**, sorted by overall scores, following the format of Table 4.

Model	Explainer	NE	SE	avg
ProtGNN+GIN	GuidedBackprop	0.80±0.21	0.55±0.04	0.68±0.12
ProtGNN+GIN	Saliency	0.62±0.29	0.72±0.15	0.67±0.05
ProtGNN+GAT	GuidedBackprop	0.77±0.22	0.54±0.08	0.65±0.11
ProtGNN+GIN	GNNE explainer	0.81±0.21	0.49±0.02	0.65±0.16
ProtGNN+GCN	GuidedBackprop	0.75±0.23	0.52±0.09	0.63±0.12
ProtGNN+GCN	GNNE explainer	0.67±0.25	0.51±0.04	0.59±0.08
ProtGNN+GAT	GNNE explainer	0.61±0.25	0.53±0.05	0.57±0.04
ProtGNN+GAT	PGExplainer	0.58±0.31	0.54±0.13	0.56±0.02
GIN	GNNE explainer	0.57±0.12	0.52±0.03	0.54±0.03
ProtGNN+GAT	Saliency	0.51±0.33	0.57±0.11	0.54±0.03
GAT	GNNE explainer	0.57±0.06	0.50±0.00	0.53±0.03
ProtGNN+GCN	GraphMaskExplainer	0.55±0.05	0.50±0.00	0.52±0.02
ProtGNN+GIN	IntegratedGradients	0.51±0.29	0.52±0.08	0.52±0.00
ProtGNN+GAT	GraphMaskExplainer	0.53±0.07	0.50±0.00	0.52±0.02
ProtGNN+GIN	InputXGradient	0.62±0.29	0.41±0.07	0.52±0.10
GIN	GuidedBackprop	0.37±0.11	0.65±0.15	0.51±0.14
GCN	GraphMaskExplainer	0.51±0.07	0.49±0.00	0.50±0.01
GIN	Deconvolution	0.45±0.16	0.55±0.18	0.50±0.05
ProtGNN+GCN	Deconvolution	0.46±0.21	0.53±0.13	0.50±0.04
GAT	GraphMaskExplainer	0.49±0.06	0.50±0.00	0.50±0.00
ProtGNN+GAT	InputXGradient	0.49±0.33	0.49±0.03	0.49±0.00
ProtGNN+GAT	Deconvolution	0.39±0.27	0.57±0.10	0.48±0.09
GIN	InputXGradient	0.39±0.18	0.56±0.10	0.48±0.08
GCN	Deconvolution	0.47±0.25	0.48±0.17	0.47±0.00
GAT	Saliency	0.39±0.30	0.56±0.12	0.47±0.09
ProtGNN+GCN	Saliency	0.42±0.30	0.52±0.14	0.47±0.05
ProtGNN+GIN	Deconvolution	0.37±0.17	0.57±0.08	0.47±0.10
GIN	Saliency	0.33±0.17	0.61±0.11	0.47±0.14
GIN	IntegratedGradients	0.35±0.17	0.57±0.17	0.46±0.11
GAT	Deconvolution	0.34±0.25	0.57±0.14	0.46±0.12
GAT	InputXGradient	0.34±0.25	0.57±0.14	0.46±0.12
GAT	GuidedBackprop	0.34±0.25	0.57±0.14	0.46±0.12
GAT	ShapleyValueSampling	0.33±0.27	0.57±0.12	0.45±0.12
GAT	IntegratedGradients	0.33±0.25	0.58±0.13	0.45±0.12
GCN	GuidedBackprop	0.35±0.24	0.55±0.08	0.45±0.10
ProtGNN+GCN	PGExplainer	0.38±0.31	0.52±0.11	0.45±0.07
ProtGNN+GCN	InputXGradient	0.40±0.31	0.48±0.03	0.44±0.04
GCN	GNNE explainer	0.37±0.25	0.50±0.04	0.44±0.06
GIN	GraphMaskExplainer	0.36±0.05	0.50±0.00	0.43±0.07
ProtGNN+GIN	GraphMaskExplainer	0.35±0.06	0.51±0.00	0.43±0.08
GCN	IntegratedGradients	0.28±0.16	0.55±0.11	0.42±0.14
GCN	InputXGradient	0.26±0.19	0.55±0.12	0.41±0.14
GIN	ShapleyValueSampling	0.22±0.11	0.55±0.12	0.39±0.17
GCN	Saliency	0.22±0.15	0.55±0.13	0.38±0.16
GCN	ShapleyValueSampling	0.23±0.17	0.53±0.12	0.38±0.15
ProtGNN+GIN	ShapleyValueSampling	0.23±0.27	0.53±0.05	0.38±0.15
ProtGNN+GCN	IntegratedGradients	0.21±0.25	0.50±0.08	0.35±0.14
ProtGNN+GIN	PGExplainer	0.21±0.20	0.46±0.05	0.33±0.13
ProtGNN+GAT	IntegratedGradients	0.17±0.29	0.48±0.05	0.33±0.15
GAT	PGExplainer	0.25±0.21	0.40±0.14	0.32±0.07
ProtGNN+GCN	ShapleyValueSampling	0.14±0.25	0.51±0.07	0.32±0.19
ProtGNN+GAT	ShapleyValueSampling	0.13±0.30	0.48±0.04	0.31±0.18
GCN	PGExplainer	0.15±0.10	0.46±0.16	0.30±0.16
GIN	PGExplainer	0.05±0.06	0.37±0.16	0.21±0.16

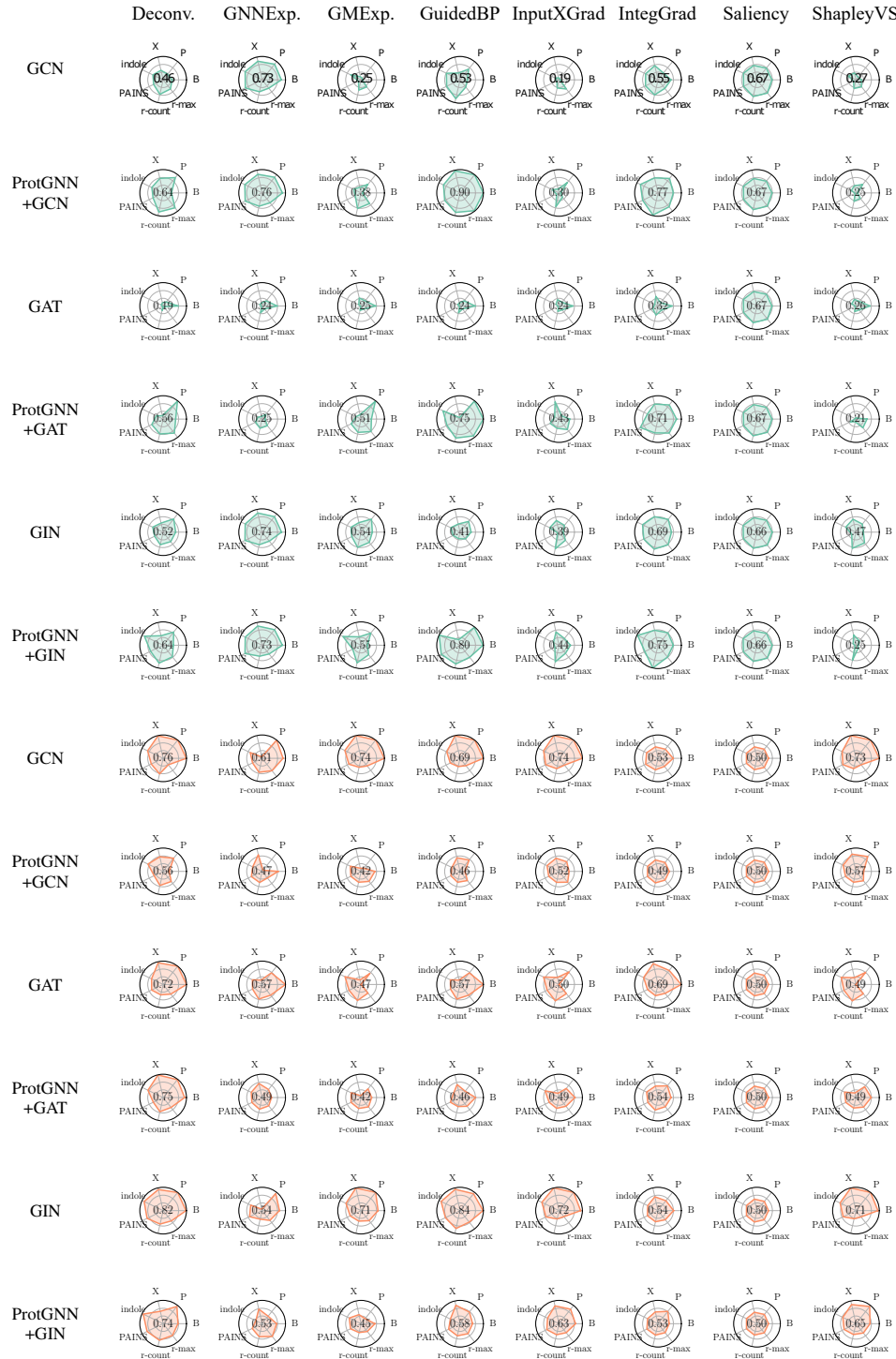


Figure 7: Evaluation of **node explanations** for all model-explainer combinations. Null explanation results are shown in green, and subgraph explanation results are displayed in orange. Overall average scores for each method are displayed in the center.

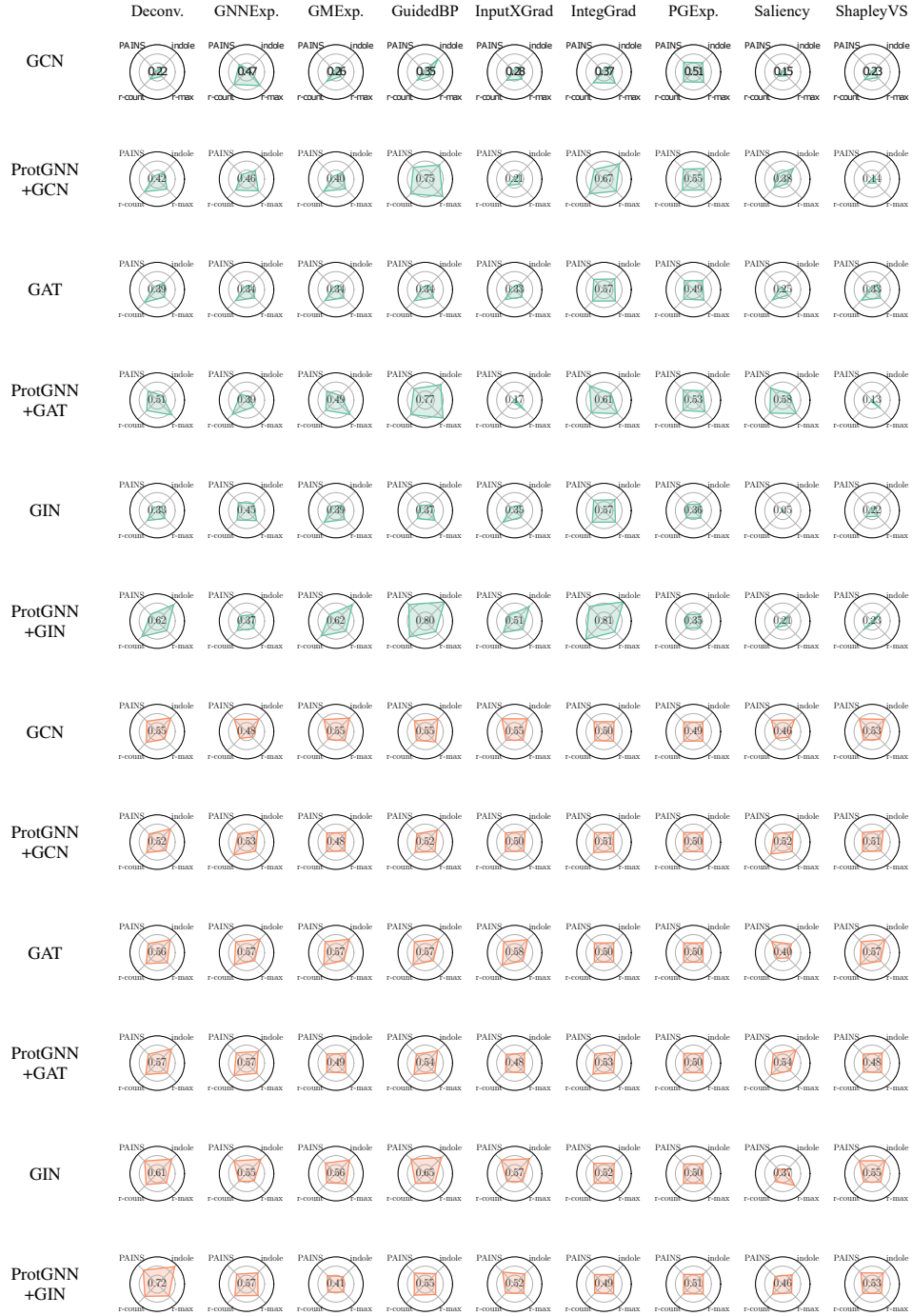


Figure 8: Evaluation of **edge explanations** for all model-explainer combinations. Null explanation results are shown in green, and subgraph explanation results in orange. Overall average scores for each method are displayed in the center.

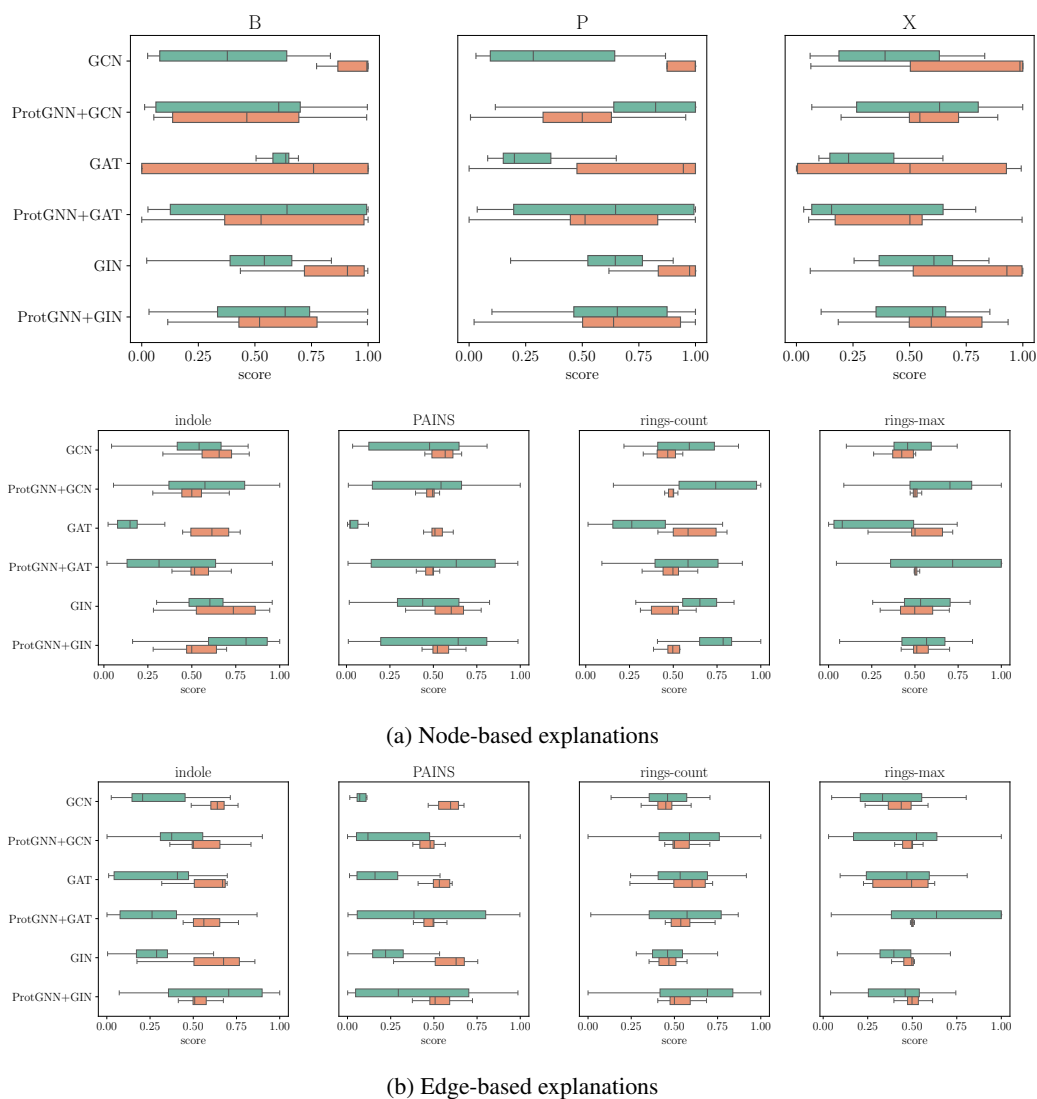


Figure 9: Boxplots showing the distribution of explanation quality across different explainers for each model. Results are aggregated per model, highlighting that some models are inherently more difficult to explain than others.

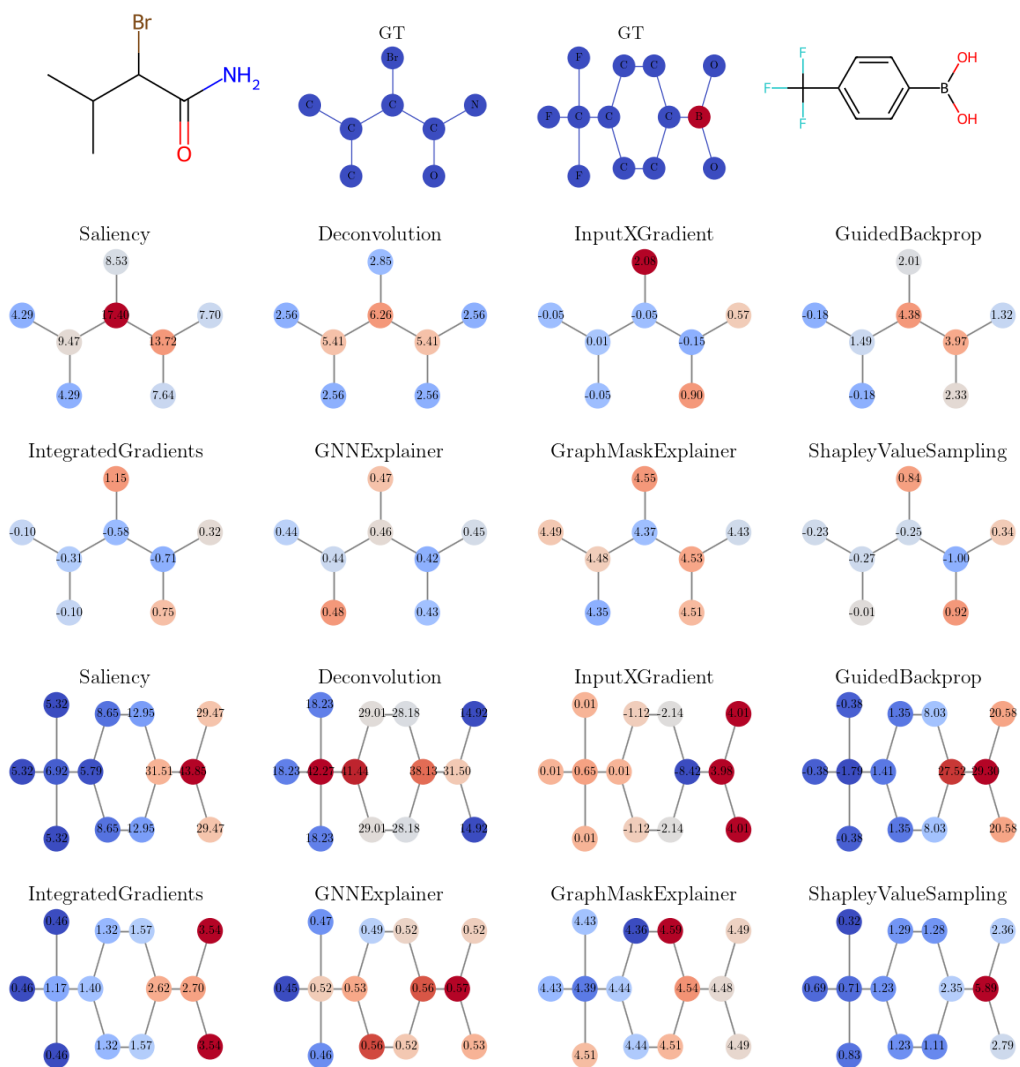


Figure 10: Node-level explanation examples on graphs from different classes in the **B** task, using the GIN model and different explanation methods.

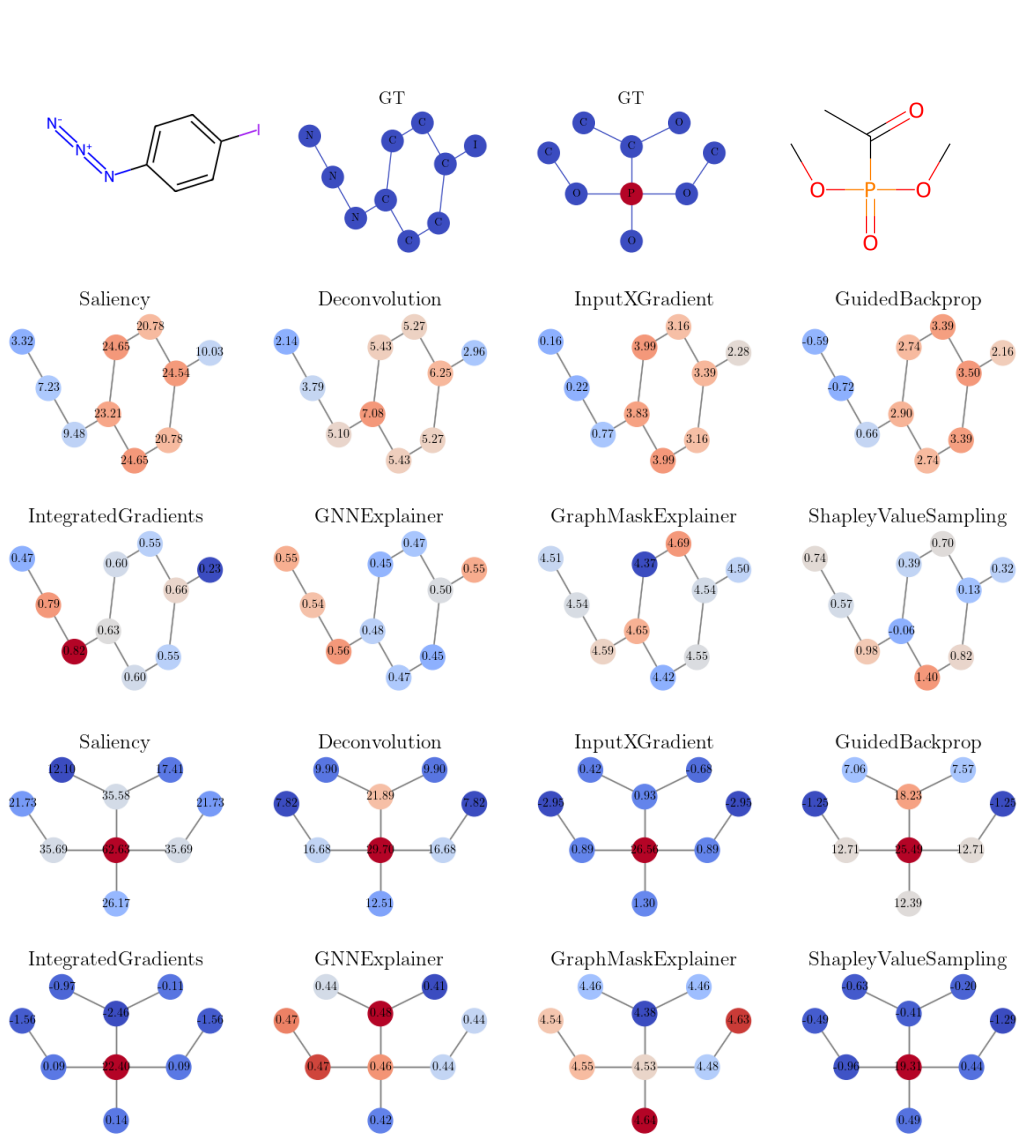


Figure 11: Node-level explanation examples on graphs from different classes in the **P** task, using the GIN model and different explanation methods.

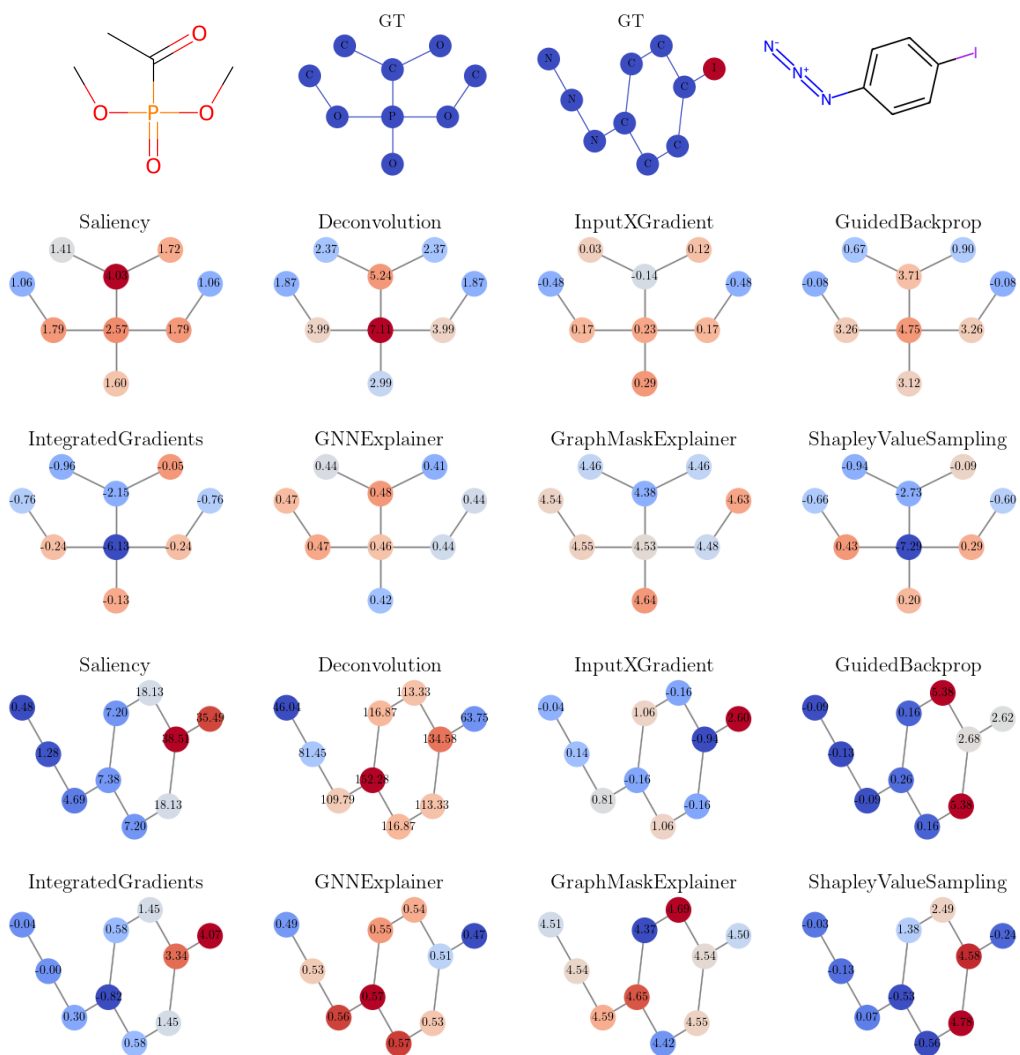


Figure 12: Node-level explanation examples on graphs from different classes in the X task, using the GIN model and different explanation methods.

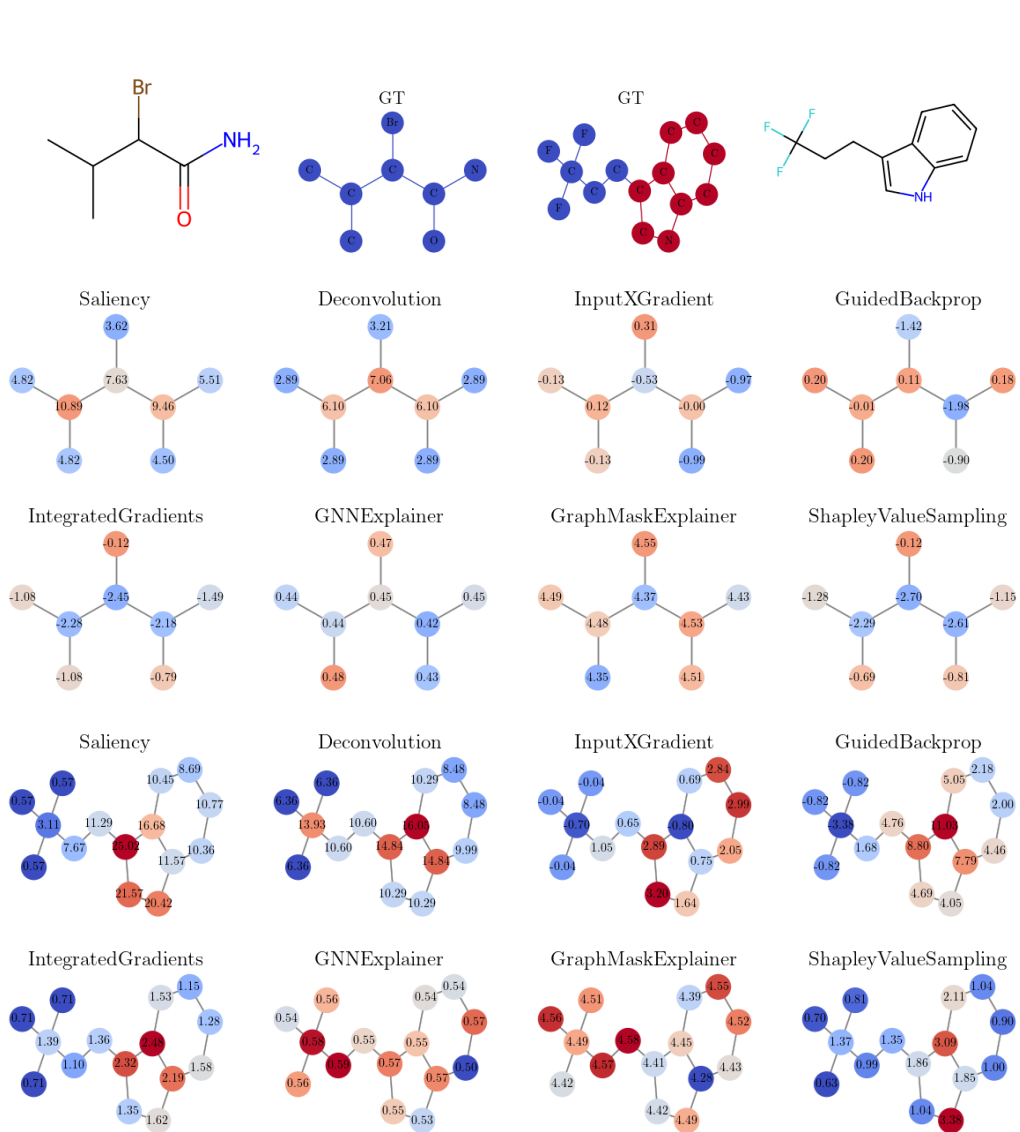


Figure 13: Node-level explanation examples on graphs from different classes in the **indole** task, using the GIN model and different explanation methods.

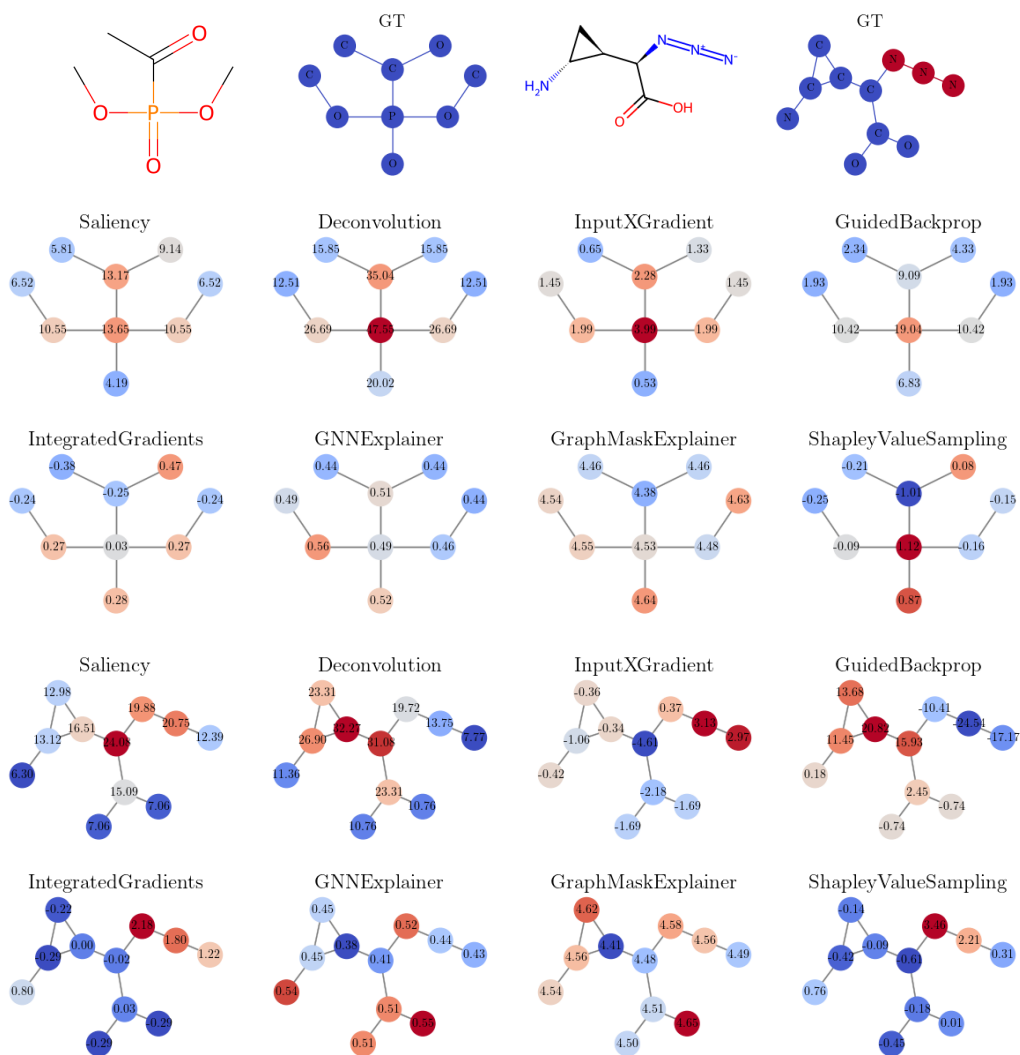


Figure 14: Node-level explanation examples on graphs from different classes in the **PAINS** task, using the GIN model and different explanation methods.

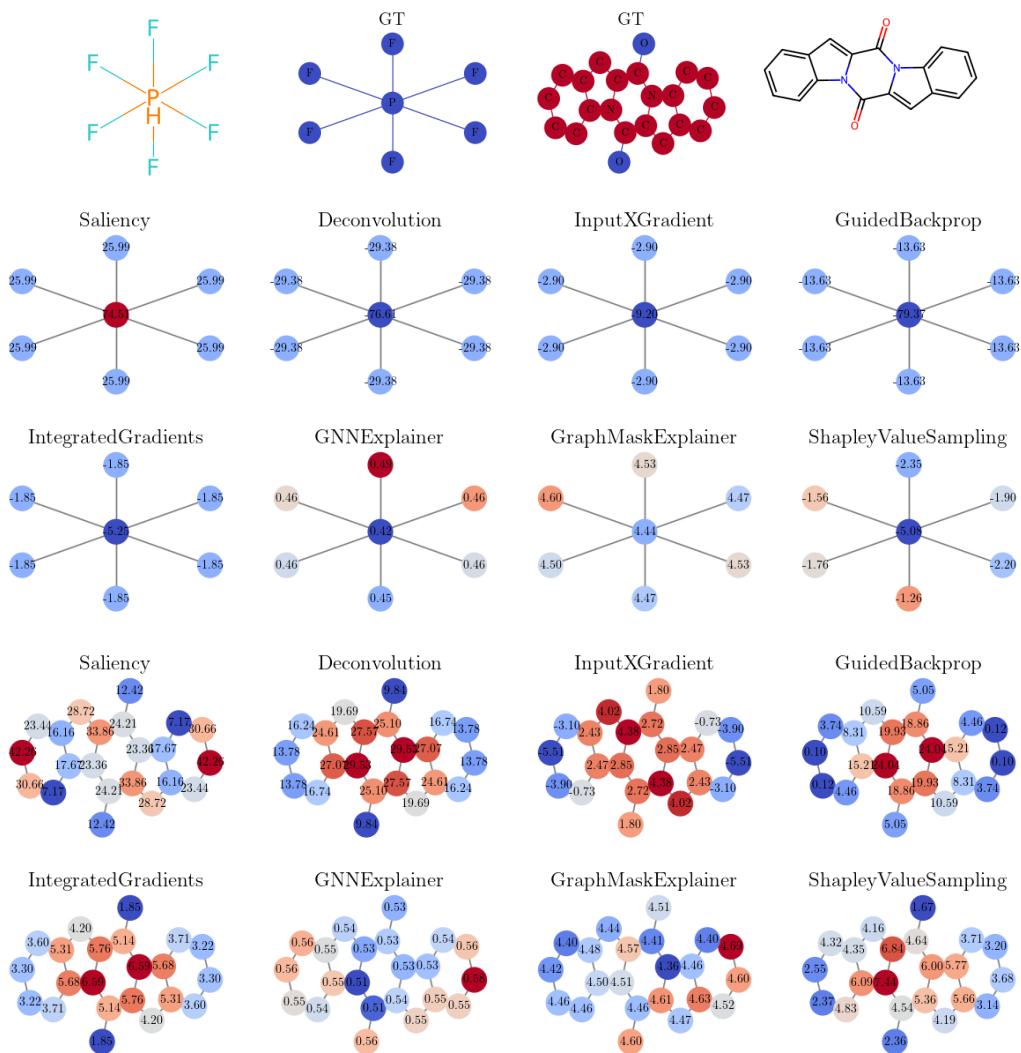


Figure 15: Node-level explanation examples on graphs from different classes in the **rings-count** task, using the GIN model and different explanation methods.

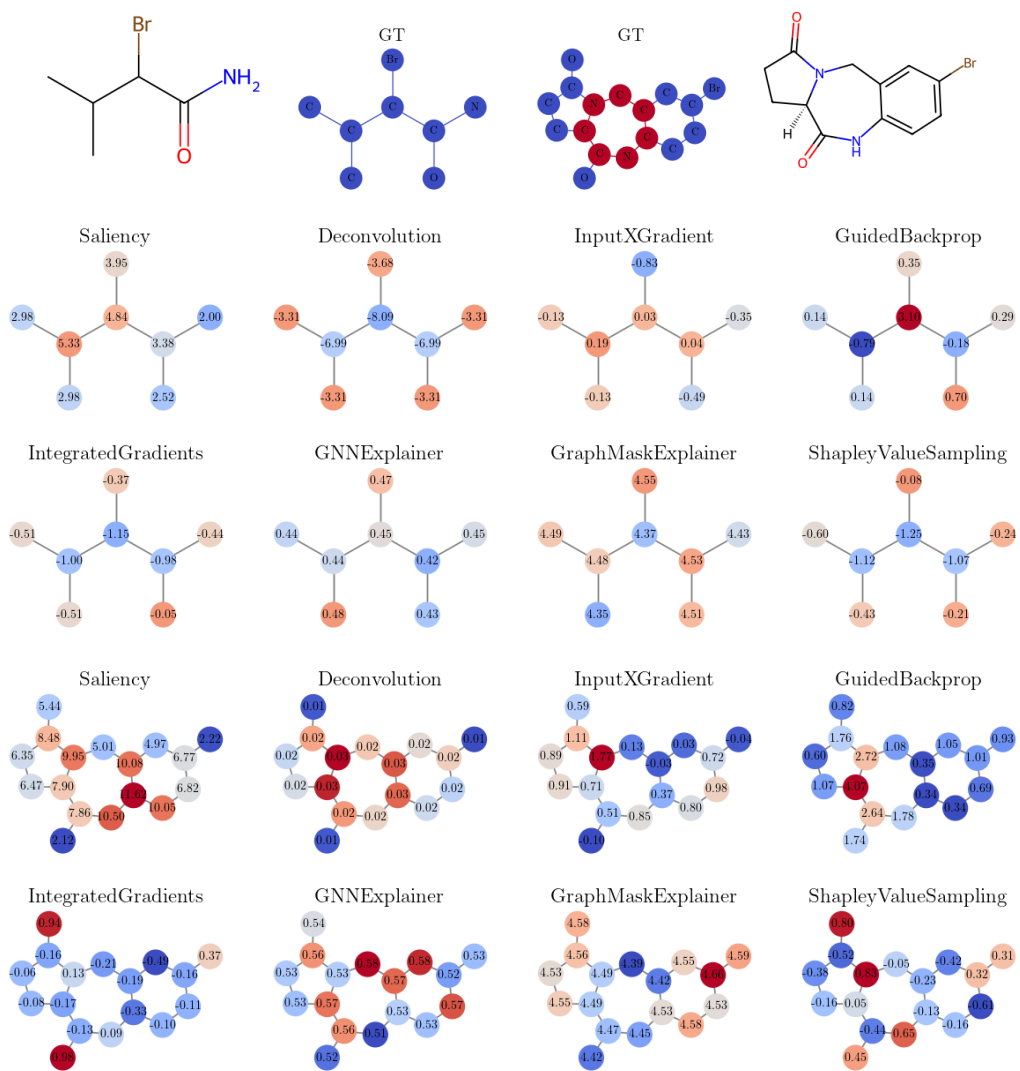


Figure 16: Node-level explanation examples on graphs from different classes in the **rings-max** task, using the GIN model and different explanation methods.